Quantum-induced symmetry breaking in the deuterated dihydroanthracenyl radical

Olha Krechkivska,[1] Callan M. Wilcox,[1] Klaas Nauta,[1] Scott H. Kable[1] and Timothy W. Schmidt[1,2*]

1. School of Chemistry, UNSW Sydney, NSW 2052, Australia

2. ARC Centre of Excellence in Exciton Science, Australia

*To whom correspondence should be addressed; E-mail: timothy.schmidt@unsw.edu.au.

Abstract

The hydrogen-atom adduct with anthracene, 9-dihydroanthracenyl radical ($C_{14}H_{11}$), and its deuterated analogue, have been identified by laser spectroscopy coupled to time-of-flight mass spectrometry, supported by time-dependent density functional theory calculations. The electronic spectrum of 9-dihydroanthracenyl radical exhibits an origin band at $19115\,cm^{-1}$ and its ionization energy was determined to be 6.346(1) eV. The spectra reveal a low-frequency vibrational progression corresponding to a mode described by a butterfly-inversion. In the deuterated analogue, a zero-point-energy imbalance along this coordinate is found to lead to a doubling of the observed spectral lines in the progression. This is attributed to quantum-induced symmetry breaking as previously observed in isotopologues of CH_5^+.

1

1 Introduction

Polcyclic aromatic hydrocarbons (PAHs) are of broad general interest. They are considered by some to be nano-graphenes,[1, 2] are by-products of combustion,[3, 4] and pose significant environmental health risks.[5] There is also substantial evidence for their widespread abundance in astrophysical environments. While the first definitive identification of an interstellar aromatic species was reported only in 2018,[6] PAHs have long been held responsible for several infrared emission features observed in post asymptotic giant branch stars, young stellar objects and galactic nuclei.[7]

Given the abundance of hydrogen atoms in the interstellar medium (ISM), it is of interest to study the interaction of hydrogen with prototypical PAHs. Indeed, PAHs are thought to act as catalysts for the formation of molecular hydrogen in Space.[8–11] Reversible addition of H to PAHs provides a pathway to deuterium enrichment in the ISM.[12] Sandford and co-workers concluded that PAHs can be enriched with deuterium by ion-molecule reactions in dense molecular clouds, and PAHs represent the largest reservoir for D enrichment of all ion-molecule reactions.

The radicals formed by H-addition to PAHs are resonance-stabilized.[13] This stabilization of radicals allows their concentrations to build up in reactive and harsh environments, such as in combustion[4, 14, 15] and are postulated to occur in the interstellar medium.[16] The association of hydrogen with benzene breaks aromaticity and forms the cyclohexadienyl radical (C_6H_7),[17] an important class of intermediate involved in many processes, such as the atmospheric oxidation of benzene.[18, 19] Addition of hydrogen to naphthalene can occur at one of two unique locations on the ring, forming the 1- and 2-dihydronaphthyl radicals ($C_{10}H_9$).[20–22] The spectroscopy and thermochemistry of the 1- and 2-dihydronaphthyl radicals were explored by Zwier and co-workers to aid in the photochemical models of PAH formation in the

atmosphere of Titan.[23]

There has been little attention given to the H-adduct with anthracene, the dihydroanthracenyl radical ($C_{14}H_{11}$, H-An). Maier and co-workers observed a dihydroanthracenyl radical in a neon matrix.[24] They observed a broad absorption feature in the ultraviolet with an origin at 326 nm. The location of the additional hydrogen on the anthracene scaffold was not determined, with the authors reporting that the spectrum may relate to H-addition at the 1 and or 9-positions.

In this work, we identify the 9-dihydroanthracenyl radical by resonance-enhanced ionization spectroscopy supported by density functional theory calculations. As in previous work,[22] we also added a deuterium atom and find that a zero-point-energy imbalance along an out-of-plane bending coordinate leads to quantum-induced symmetry-breaking, as previously observed in CH_5^+,[25] with striking spectroscopic consequences.

2 Experimental

The experimental apparatus and methods have been described previously.[22, 26] Briefly, a sample of anthracene was heated in the range $75 - 100°$C before a pulsed discharge nozzle, which was held $\sim 10°$C higher to prevent condensation of the sample. A gas mixture of argon and (heavy) water was passed through the sample container, collecting the vapour of anthracene. The (heavy) water was heated externally to $50°$C.

A discharge of 2.1 kV was struck for $130\,\mu$s during the gas expansion, with current limited by a $20\,k\Omega$ ballast resistor. Following the discharge, the mixture was supersonically expanded into a differentially-pumped vacuum chamber and the coldest part of the expansion was admitted through a 2 mm skimmer. To search for the H and D-adducts of anthracene, a resonant 2-color 2-photon ionization (R2C2PI) scheme was employed. An ionisation source of $\sim$290 nm was used. The m/z 179 and 180 signals, (corresponding to H-An and D-An), were recorded as a function of excitation wavelength.

The ionization energy of the radicals was measured by fixing the excitation laser to the origin (or a low-lying vibrational band) of the radical's electronic excitation, and scanning the ionization laser. The excited-state lifetime of the H-adduct was obtained by fixing the timing of the ionization pulse, and scanning the timing of the preceding excitation laser pulse. The trace was fit to an exponential decay.

Hole-burning experiments were conducted on the deuterium adduct, to confirm the commonality of the spectral carrier of individual excitation bands. With the excitation laser fixed on a particular band, a hole-burning laser was introduced about 500 ns prior, to remove population from the ground state and thus deplete the resonant ionization signal. The wavelength of the hole-burning laser was scanned to reveal the excitation spectrum of the species probed by the R2C2PI experiment.
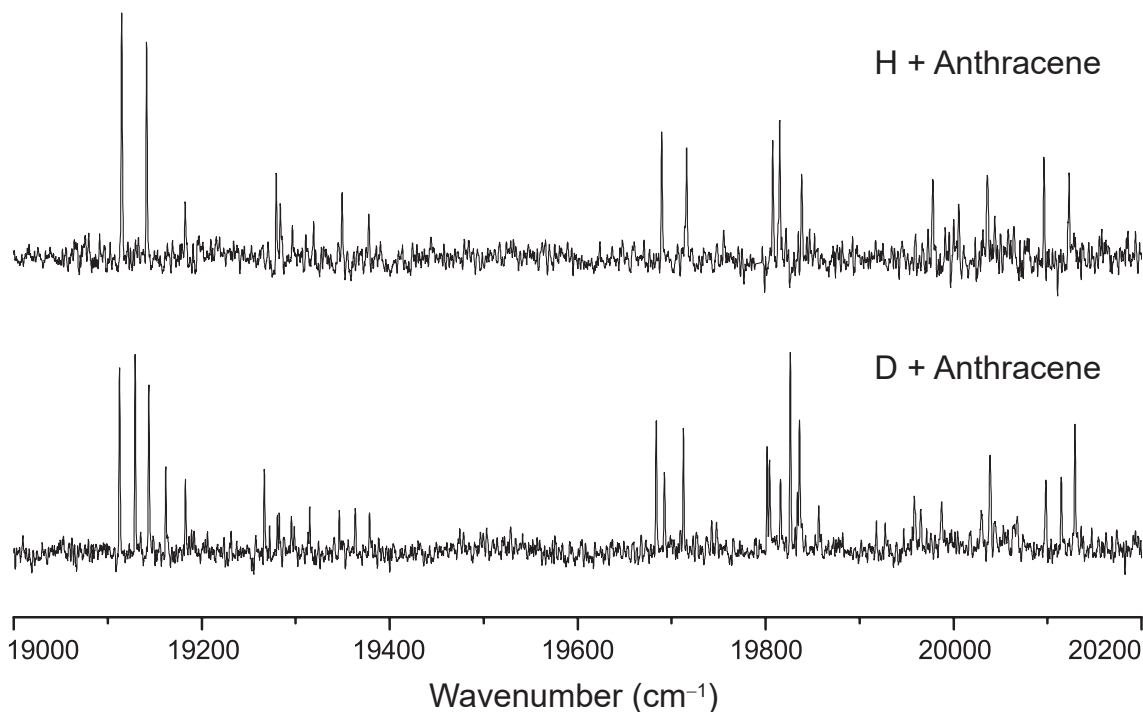

Figure 1: R2C2PI spectra of a dihydroanthracenyl radical (H-An, $C_{14}H_{11}$) and the deuterated analogue (D-An, $C_{14}H_{10}D$).

4

3   Results

R2C2PI spectra were recorded for m/z 179 and 180, corresponding to adducts of anthracene with a hydrogen or deuterium atom respectively (H-An, $C_{14}H_{11}$ and D-An, $C_{14}H_{10}D$). The spectra are plotted in Figure 1. The spectra exhibit rich vibrational structure with multiple peaks near the origin for both species.
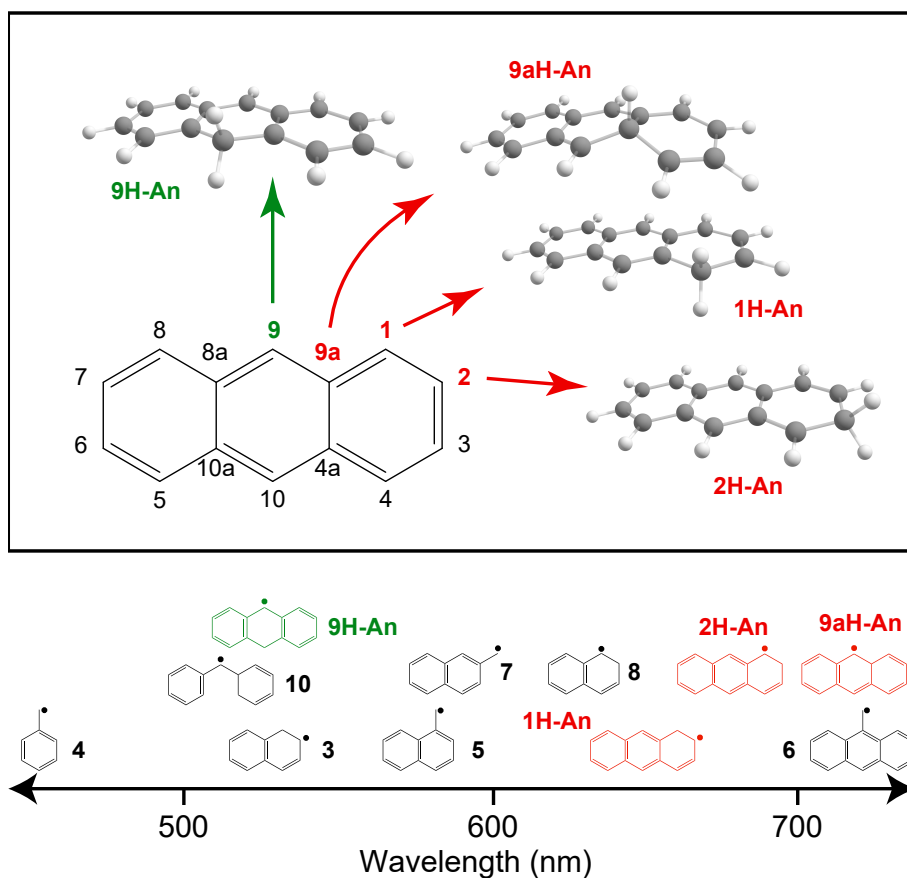

Figure 2: Numbering convention for anthracene derivatives with unique substitution locations shown in bold, pointing to structures of H-An radicals. See text for a discussion of previously observed radicals with chromophores similar to those of the four dihydroanthracenyl radical isomers.

3.1 Identification of the 9-dihydroanthracenyl radical

There are four symmetry-distinct sites at which a hydrogen atom may attach to anthracene: At the 1-, 2-, 9- and 9a-positions (Figure 2). The observed species at m/z 179 presents a putative origin band at 523 nm (19115 cm^{-1}) and we use this information to propose the identity by comparison to known spectra.

The chromophore presented by the 1-dihydroanthracenyl radical (**1H-An**) could be considered a benzannulated 1-dihydronaphthyl radical (**3** in Figure 2). This radical, which has a phenylallyl-type chromophore, was observed by Zwier and co-workers to absorb at 528 nm.[23] However, benzannulation shifts the absorption to longer wavelength.[13] For instance, benzyl radical (**4**) absorbs at 454 nm, 1-naphthylmethyl radical (**5**) absorbs at 580 nm,[27] and 9-anthracenylmethyl (**6**) absorbs at 727 nm.[28] As such, we would expect 1-dihydroanthracenyl radical to absorb some ~130 nm to longer wavelength than the observed 1-hydronaphthyl origin, i.e. near 658 nm.

The 2-dihydroanthracenyl radical (**2H-An**) chromophore is similar to the 2-naphthylmethyl radical (**7**) substituted with an *ortho* vinyl group. Vinyl substitution tends to shift absorptions to lower wavenumber (longer wavelength) by about 2500 cm^{-1}.[13] A vinyl-substituted 2-naphthylmethyl radical chromophore would therefore be expected to absorb redward of 584 nm.[27] The 2-dihydroanthracenyl radical may also be considered a benzannulated 2-dihydronaphthyl radical (**8**). The latter radical is thought to absorb near 636 nm,[29] and a benzannulated version would almost certainly absorb redward of that figure.

The 9a-dihydroanthracenyl radical (**9aH-An**) is not expected to be particularly stable on account of the induced ring strain, and the equivalent H adduct with naphthalene has not been observed.[20] Such a radical would exhibit a nine-membered π-chromophore with benzannulation. The pentadienyl chromophore absorbs near 514 nm,[30] which is ~106 nm redward of the three-membered allyl chromophore.[31] The nine-membered π-chromophore on its own would

6

therefore be expected to absorb at some 726 nm, far to the red of the observed spectrum.

The 9-hydroanthracenyl radical (**9H-An**) exhibits a very similar chromophore to the diphenyl-methyl (α-phenylbenzyl) radical (**10**), which has been studied previously.[32] Shibuya and co-workers assigned the origin of this radical to a feature observed at 516 nm (19370 cm^{-1}), with extensive Franck-Condon activity observed in torsional modes. The close proximity to the absorption position of the presently observed spectrum strongly suggests the identity to be 9-hydroanthracenyl radical.

Photo-ionization spectra were obtained for each of the peaks in the origin regions of the H-An and D-An spectra. The results are displayed in Figure 3. The top two spectra result from exciting the origin and the first successive transitions in the H-adduct spectrum, and are labelled h_a and h_b. The point of intersection between the baseline and the ionization onset is more clearly defined for h_a, and so we have used this spectrum to determine the ionization energy. This range encompasses the value obtained by ionizing through h_b and can be considered consistent. In previous experiments we determined that for similar sized radicals, the finite electric field in the extraction region was responsible for a depression of the observed IE of 7 meV. As such, our recommended value is 6.3462(10) eV.[33]

Time-dependent density functional theory calculations were performed to support the above identification of the spectral carrier. (TD)-B3LYP calculations were carried out using the Gaussian 16 suite of programs[34] and the 6-311+G(d,p) basis set. The adiabatic (and ZPE corrected) ionization energies of the 1H-An, 2H-An, 9aH-An and 9H-An isomers were also calculated at the B3LYP/6-311+G(d,p) level of theory, and the results are reported in Table 1. All four isomers are predicted to have similar ionization energies and, characteristic of the B3LYP/6-311+G(d,p) level of theory, the values are lower than the observed value.[33, 35]

For a range of resonance-stabilized radicals, Troy reported that the B3LYP/6-311+G(d,p) adiabatic ionization energies underestimated experiment by a deviation of 0.14(7) eV.[35] By
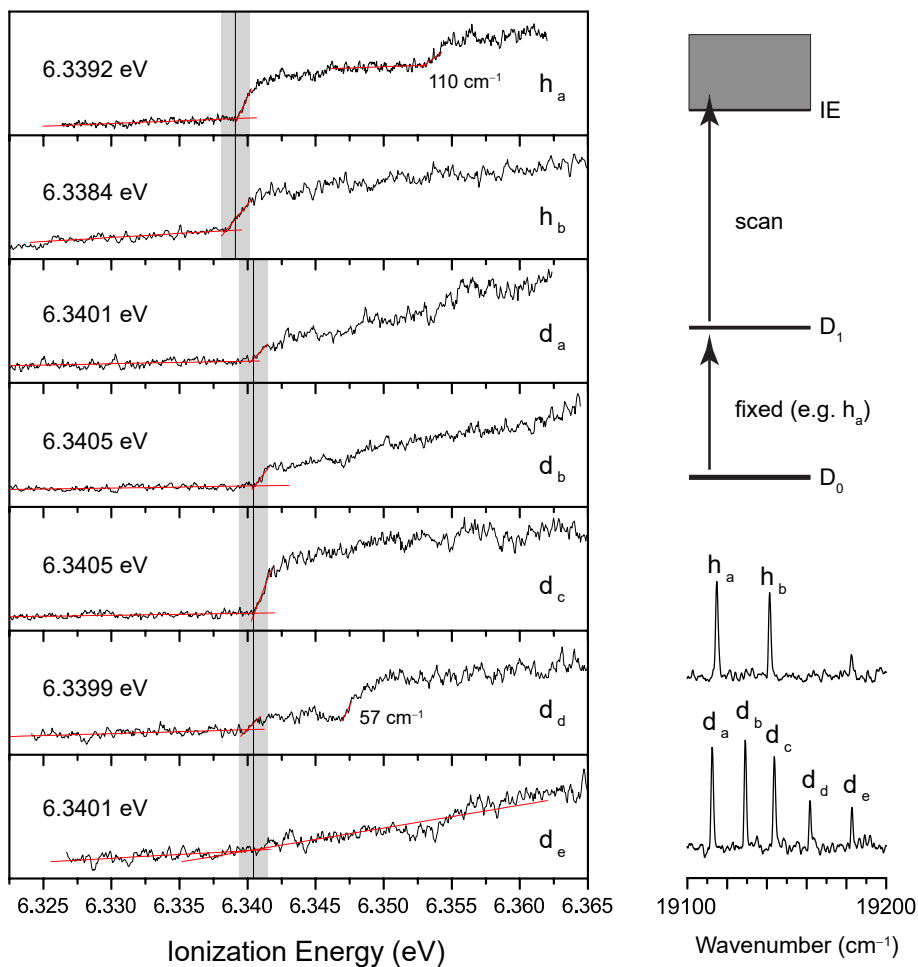
Figure 3: Photo-ionization spectra of the H-An (h_a and h_b) and D-An radicals (d_a to d_e), with the first excitation through the band indicated. Top right is a schematic of the ionization scheme. The reported ionization energy in the text and Table 1 is corrected by +0.007 eV to account for the finite electric field in the extraction region of the spectrometer.[33]

adding the 0.14(7) eV to the calculated adiabatic energies, we obtain our best calculated estimates for the ionization energies of the various isomers. All but 9aH-An radical have calculated IEs consistent with the experimentally observed value of 6.346 eV. As such we cannot use the ionization energy alone as a way to discriminate between the isomers. However, they are consistent with the carrier being assigned to an H-An species (other than 9aH-An).

The calculated relative energies of 1H-An, 2H-An, 9aH-An and 9H-An are given in Ta-

ble 1. The 9H-An isomer is the most energetically favourable to form, by 27.7, 45.6 and 136.8 kJ mol^{-1} compared to addition at the 1-, 2- and 9a- positions respectively. While an electric discharge is capable of generating higher energy isomers,[26] the low energy calculated for 9H-An supports its assignment as the observed carrier.

The adiabatic $D_1 \leftarrow D_0$ excitation wavelengths for the 1H-An, 2H-An and 9H-An isomers were also calculated at the TD-B3LYP/6-311+G(d,p) level, including their respective zero-point energy corrections (Table 1). The TD-B3LYP geometry optimization in the D_1 state of the 9aH-An isomer failed to converge. The calculated absorption wavelengths are consistent with the assertions in Figure 2, which were based on comparing chromophores.

The observed H-An electronic origin transition is ascribed to the first peak in the R2C2PI spectrum, at 19115 cm^{-1}. No bands were observed to the red of this transition. The calculated $D_1 \leftarrow D_0$ transition for the 9H-An isomer, at 20101 cm^{-1}, is to slightly higher energy than the observed value, with a discrepancy of 986 cm^{-1}. The 1H-An and 2H-An isomers are calculated to absorb some 2462 cm^{-1} and 3591 cm^{-1} lower in energy, respectively, than 9H-An. On the basis of the observed origin band position and the relative isomer energies, we assign the observed spectrum to the 9-dihydroanthacenyl radical, 9H-An.

3.2 Spectral Hole-burning

With the identity of the 9H-An radical secure, we note a curious difference between the deuterium and hydrogen-adducts in Figure 1. The higher resolution spectra of the origin regions (see Figure 3) reveal a halving of the observed low frequency mode upon deuteration – something which is not possible due to the mass difference alone. To check that all bands originate in a single isotopologue, and not from scrambling of the D-position, we performed hole-burning experiments.

In order to perform a hole-burning experiment and remove population from the $v = 0$ level,

Table 1: Calculated (TD)-B3LYP/6-311G+(d,p) Energies, Excitation Wavelengths and Ionization Energies of $C_{14}H_{11}$ Isomers

Isomer	Rel. Energy^a (kJ mol^{-1})	Excitation (nm)	IE^{a,b} (eV)
1H-An	27.7	600	6.38(7)
2H-An	45.6	644	6.34(7)
9H-An	0	497	6.29(7)
9aH-An	136.8	unconverged	6.16(7)
Recommended		523	6.3462(10)^c

a ZPE corrected

b Adiabatic, corrected by +0.14(7) eV (see text)[35]

c Corrected by +0.007 eV to account for the finite electric field in the extraction region of the spectrometer[33]
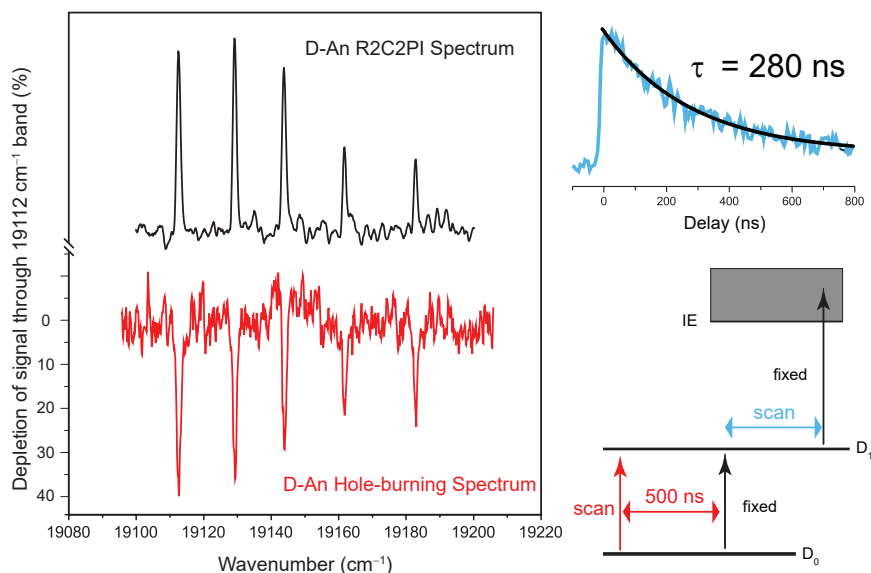

Figure 4: Hole-burning spectrum of the D-An radical probed through the origin band. As all features are present in both spectra, we can conclude that they belong to the same ground state species. At top right is the scan of the excitation-ionization delay which reveals the excited state lifetime. At bottom right is a schematic of the lifetime and hole-burning experiments.

the hole-burning laser pulse must precede the ionization scheme by a long enough delay that the excited state decays such that it is no longer readily ionized. To this end, we performed

an experiment in which the delay between the excitation and ionization laser pulses is scanned from negative to long positive delays. The results are plotted in Figure 4, and the trace is fit to a single exponential decay with a time constant of 280 ns. In the hole-burning experiment, the hole-burning pulse was timed 500 ns prior to the ionization scheme.

Figure 4 displays two spectra. At top is the R2C2PI spectrum of the D-An electronic origin region. Fixing the R2C2PI scheme to the $19112\,\mathrm{cm}^{-1}$ origin, the hole-burning laser is scanned across the spectral range. Bands that exhibit depletion belong to the same lower state (and therefore species) as the origin. There is a clear and definitive depletion of all five bands in the D-An R2C2PI spectrum and therefore all five bands belong to the same spectral carrier and lower state as the band at $19112\,\mathrm{cm}^{-1}$. This confirms that H-D exchange does not occur to an observable extent, and that there is only one isotopologue responsible for the D-An spectrum. We assign this to the 9D-An radical.

3.3   Spectral Assignments

The origin regions of both the 9H-An and 9D-An radicals exhibit a progression in a low-frequency, anharmonic mode. This progression is reprised as a motif built onto many of the vibronic features, which is particularly clear for the two pairs of 9H-An bands near $19700\,\mathrm{cm}^{-1}$ and $20100\,\mathrm{cm}^{-1}$.

To commence a spectral assignment, we performed excited-state frequency calculations at the TD-B3LYP/6-311+G(d,p) level. A full list of calculated frequencies is provided in the Supporting Information. For ease of comparison to experiment, we scale the calculated frequencies by 0.97.[26] Both the optimized (TD)-B3LYP/6-311+G(d,p) geometries of the D_0 and D_1 states have the $>CH_2$ group puckered slightly out of plane, reducing the point-group symmetry from C_{2v} to C_s. As such, we have labelled and arranged the calculated modes according to the Mulliken convention in this point group. The lowest-frequency calculated mode, $\nu_{37} = 36\,\mathrm{cm}^{-1}$, is
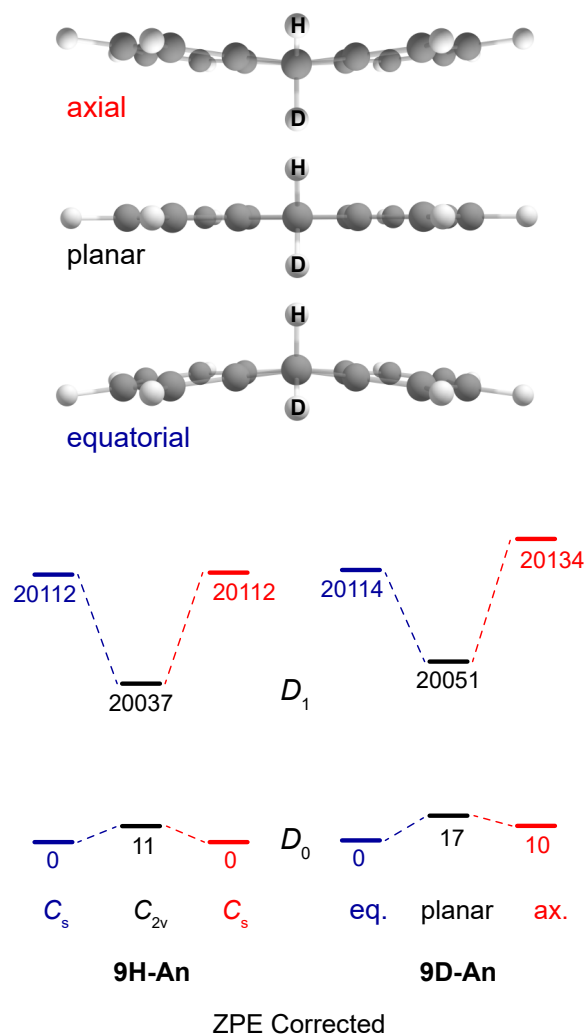
Figure 5: Top: Illustration of the butterly mode, ν_{37}, highlighting the difference in the D position. Bottom: The ZPE-corrected (TD)-B3LYP potential energy surface of the butterly mode.

a "butterfly" motion. At the C_{2v} saddle point, this mode is of b_1 symmetry with an imaginary frequency of $43\mathrm{i}\,\mathrm{cm}^{-1}$. The next lowest calculated frequency is $\nu_{69} = 81\,\mathrm{cm}^{-1}$, and is a'' in the C_s point group making it unlikely to have any intensity in single quanta (note that the mirror plane is perpendicular to the molecular framework). The first band encountered above the origin in the spectrum of 9H-An lies at just $+26.6\,\mathrm{cm}^{-1}$. As such, we attribute the low frequency

progression to ν_{37}.

Comparing the 9H-An and 9D-An origin regions, it would appear that there is a doubling of the number of observed bands. A halving of the frequency is not expected, nor is it supported by calculations. We calculated the excited-state frequencies of the two C_s 9D-An isotopomers, with the D position axial or equatorial. Both have ν_{37} at about $35\,\mathrm{cm}^{-1}$, similar to 9H-An. But, the results of hole-burning experiments rule out that the extra bands appear due to two isotopomers. We therefore conclude that there are lines missing in the spectrum of 9H-An. This implies a selection rule for the 9H-An isomer possibly arising from a completely symmetric ground state wavefunction in C_{2v} to an excited state with a low or absent barrier to inversion. In this case, the low frequency progession in 9H-An is assigned to 37_0^{2v}.

It is interesting at this point to draw a comparison between our spectra and the $S_1 \leftarrow S_0$ spectrum of 9,10-dihydroanthracene.[36–38] This molecule is strongly bent in both ground and excited states, and shows a clear, lengthy Franck-Condon progression in the low-frequency butterfly motion. The progression in the excitation spectrum of dihydroanthracene is highly anharmonic, due to the double-well in the excited state. However, for this molecule the ground state is essentially degenerate since the barrier separating the two wells is $>600\,\mathrm{cm}^{-1}$. This means all transitions, between even-to-even and odd-to-odd states, are seen, comprising what is essentially a bent-to-bent Franck-Condon envelope with no missing bands. Contrastingly, the doubling of the number of observed transitions upon deuteration at the 9-position of 9H-An implies that we have a single symmetric ground state in C_{2v}, and are missing the odd-levels in the excitation spectrum of 9H-An. The present radical should therefore be considered a C_{2v} species. For 9D-An, the asymmetry induced by the deuterium atom skews the zero-point corrected potential in both ground and excited states, returning the spectrum to the appearance of a bent-bent transition. The zero-point corrected energies at the Born-Oppenheimer minima and the C_{2v} transition states are plotted in Figure 5. It is interesting to note that the zero-point

energies are lower for the C_{2v} geometry in the excited state than for the Born-Oppenheimer minima. The skewed nature of the 9D-An potential is clearly predicted. We return to this important point in the discussion.

Given the anharmonic nature and low frequency of ν_{37}, we opted to model this coordinate empirically. Assuming that the peaks at +26.6 and +67.7 cm^{-1} represent excitations of even quanta of the butterfly mode, we fit the spacings to a model quartic potential, similar to the method of Laane and Veguilla-Berdeca.[39, 40] Using the reduced mass of 3.4 amu of ν_{37} taken from the TD-B3LYP calculations, the spacings of the first three bands observed in the 9H-An spectrum were well fit to a potential of the form $V(q) = -8.33q^2 + 5.81q^4$ (plotted in Figure 6, units of cm^{-1} and Å). Two level-spacings and two parameters are likely to result in a good fit, but this potential can be tested by modelling the 9D-An spectrum.

As the 9H-An molecule proceeds along the butterfly coordinate, one H moves from an equatorial position to an axial position, with the other changing in the opposite sense. These geometries are equivalent for 9H-An, but they are not for 9D-An. Deuteration does not break the symmetry of the 9H-An symmetric potential from the standpoint of the electronic energies, but the difference in the zeropoint energies of the other modes introduces an asymmetry to the double-well potential for 9D-An. The (TD)-B3LYP calculation predicts that this difference will be on the order of 10s of cm^{-1} (Figure 5).

Terms in the potential which modulate the vibrational frequency of a particular mode j, while progressing along q_{37} are of the form $V'_j = a_{37,j}q_{37}q_j^2$, where $a_{37,j} = m_j\omega_j d\omega_j/dq_{37}$. Now, in a harmonic basis for all $j \neq 37$, we may integrate over these coordinates to arrive at an effective potential

$$
\begin{aligned}
V(q_{37}) &= V_{BO}(q_{37}) + q_{37}\sum_{j\neq 37} a_{37,j}(2v_j+1)\frac{\hbar}{2m_j\omega_j} \\
&= V_{BO}(q_{37}) + q_{37}\sum_{j\neq 37} \frac{(2v_j+1)\hbar}{2}\frac{d\omega_j}{dq_{37}}
\end{aligned}
\tag{1}
$$

14

where V_{BO} is the Born-Oppenheimer potential and n_j is the number of quanta in mode j. Where $v_j = 0 \,\forall j$, this reduces to the change in the zero-point energy for all modes $j \neq 37$ along q_{37}.

Using the same model potential as for 9H-An, with a linear term of $+13.34q$ to account for an offset in the zero point energies of the two wells, the level spacing in 9D-An was matched to experiment (reduced mass from (TD)-B3LYP, 3.7 amu). To model the appearance of the intensities, the ground state potential was modelled as $V(q) = (-0.99q) - 8.30q^2 + 1.69q^4$, where the linear term is only invoked for the 9D-An radical.
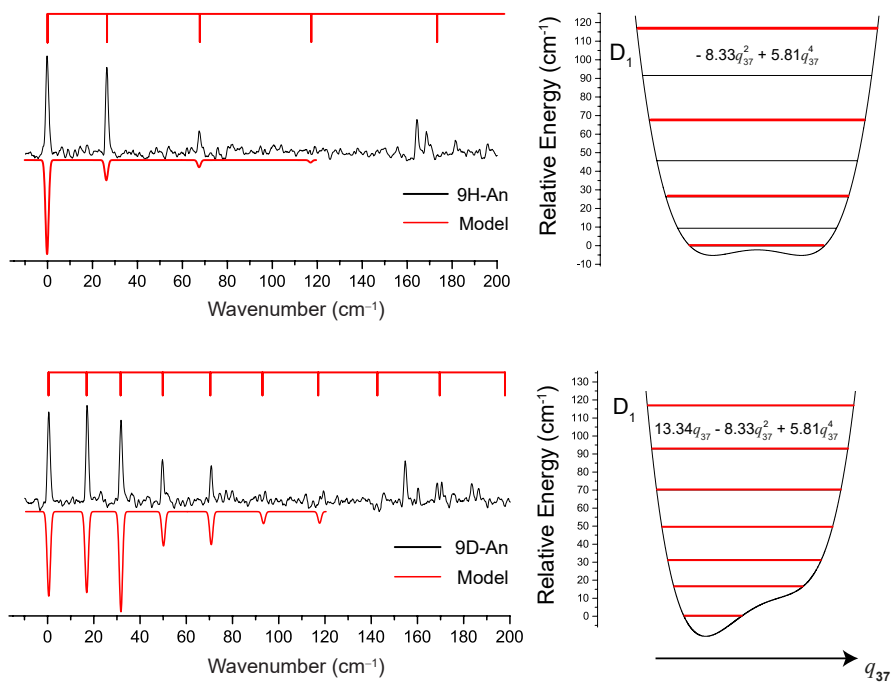

Figure 6: Model butterfly potentials and excitation spectra for the origin regions of 9H-An and 9D-An.

With the above assigment of the origin region and the activity of ν_{37} secure, we proceeded to assign the remainder of the spectra in Figure 1 using the frequencies calculated by TD-DFT. For the bulk of the spectroscopic assignment, we refer the reader to the Supporting Information, but a short list of assignments for the 9H-An isotopologue is given in Table 2. The full list of calculated frequencies at the Born-Oppenheimer minima is given in Tables S2-S4.

15

Given the appearance of selection rules in the excitation of ν_{37}, the ground state must be delocalised across the double-well potential. As such, we expect the spectrum to follow C_{2v} selection rules. For 9H-An, the frequencies were also calculated in the C_{2v} geometry to obtain their symmetries, and were correlated with the C_s frequencies by visual inspection of the normal modes. In brief, the aforementioned progressions near $19700\,\mathrm{cm^{-1}}$ and $20100\,\mathrm{cm^{-1}}$ for 9H-An mimic the origin region almost exactly and are readily assigned to the totally symmetric vibrations ν_{30} and ν_{19}. The third band in the origin progression is not always apparent in the higher vibrations, but it is also much weaker than the first two. That these two progressions should resemble the origin is due to the fact that they are fully symmetric normal modes, having a_1 symmetry in the C_{2v} saddle point geometry and a' in C_s. Another pair of bands at 19300 $\mathrm{cm^{-1}}$ is therefore also readily assigned to ν_{37} built upon a fully symmetric vibration, ν_{35}.

Several other bands visible for 9H-An in Figure 1 do not show this clear correlation with the origin progression and assignments to these are thus less secure. Nonetheless we have found reasonable assignments for these transitions by making the assumption that the only modes that show up as single quanta correlate to a_1, while b_1 modes combine with odd quanta of ν_{37}. Note that b_1 modes also correlate with a' in the bent geometry. However, we expect the C_{2v} selection rules to hold due to the proposed a_1 symmetry of the ground state. The ν_{37} potential is likely coupled to other modes, rendering the appearance of its progression sensitive to combination with these modes. Several examples are apparent in the deuterated isotopologue and we will return to this in the Discussion. The mean average deviation (MAD) between theory and calculation is $5.4\,\mathrm{cm^{-1}}$ for the scaled C_s frequencies which, considering the size of the molecule and the degree of anharmonicity associated with the floppy molecular frame, is acceptable.

Table 2: 9H-An Spectral Assignments (cm^{-1}) and Comparison to Calculations.

Observed	Relative	Assignment	Calc. C_s	Δ
19114.8	0	0_0^0	0	
19141.4	26.6	37_0^2	26.6 †	
19182.6	67.7	37_0^4	67.7 †	
19279.4	164.6	69_0^2	162.4	-2.2
19283.7	168.8	$36_0^1 37_0^1$	167.8	-1.0
19296.6	181.7	$69_0^2 37_0^2*$	189.0	
19319.1	204.2	$36_0^1 37_0^3$	203.8	
19349.4	234.5	35_0^1	232.1	-2.4
19377.9	263.0	$35_0^1 37_0^2$	258.7	
19689.5	574.7	30_0^1	565.3	-9.4
19716	601.1	$30_0^1 37_0^2$	591.9	
19755.5	640.7	$30_0^1 37_0^4$	633.0	
19807.7	692.8	$27_0^1 37_0^1$	692.8	0.0
19815.1	700.2	26_0^1	692.2	-8.0
19838.5	723.6	$26_0^1 37_0^2$	718.8	
19978	863.2	23_0^1	869.9	6.7
20005.6	890.8	$23_0^1 37_0^2$	896.5	
20036	921.2	$21_0^1 37_0^1$	927.6	6.4
20096.3	981.5	19_0^1	969.2	-12.3
20122.9	1008.1	$19_0^1 37_0^2$	995.8	

† Modelled - see text.

4 Discussion

It is evident from the previous section that deuteration at the 9-position causes a significant change in the effective structure of the radical in its D_1 state. Knowledge of the ground state is, by the nature of our experiments, limited. But, using the DFT results as a guideline, a similar deuteration effect as seen in D_1 seems likely. The DFT electronic energies place the 9-carbon distinctly out of plane for both the ground and excited states of the radical, with the excited state more puckered. However, the energy difference between the out-of-plane geometry and the C_{2v}-planar geometry is very small, and the effective structure of the 9H-An radical is therefore still essentially planar. The vibrational zero-point energy level along the butterfly mode, ν_{37}, lies at

or just above the barrier to inversion, and the associated wavefunction has equal intensities in both sides of the well.

Replacing one of the 9-carbon hydrogen atoms with a deuterium atom breaks this symmetry. Purely electronically the potential is still totally symmetric, but the vibrational frequencies of the radical are sensitive to whether the D-atom is in the axial position or in the equatorial position and the vibrational zero-point energy, for all modes except the butterfly mode, reflects this difference (see Figure 5). The symmetric double-well potential along the butterfly coordinate has therefore become an asymmetric double well, with a preponderance for the D-atom in the equatorial position, thus changing the effective (vibrationally averaged) geometry of this radical from planar to bent. While within the harmonic approximation the effect of deuteration on the butterfly vibrational motion itself is very small ($\sqrt{\mu_H/\mu_D} = 0.96$), the sum of the effect on all 68 other vibrational modes is substantial. Because this is a purely quantum mechanical effect with no classical analogue, it is termed "quantum-induced symmetry breaking".

This term was applied by Schlemmer and co-workers to the effect of deuteration on the IR spectrum of protonated methane (CH_5^+) where, for partial deuteration, there was a clear preference for the deuterium to occupy the more tightly bound CH_3 moiety within the cation.[25] In their case, the IR spectra for a given partially deuterated isotopologue could be decomposed into spectra due to all the possible isotopomers for that given isotopologue. In other words, despite the zero-point wavefunction of CH_5^+ being spread between all the possible hydrogen exchange symmetries, distinct structures corresponding to D-atoms being localised in a particular location within the molecule were distinguishable.

While the hole-burning experiment confirms that all transitions in the origin progression of 9D-An originate from a single ground state, the excitation spectrum samples both sides of the excited-state potential. Mode 30 is a case in point, where $30_0^1 37_0^1$ is observed some $7.5\,\mathrm{cm}^{-1}$ lower in energy than expected based on the origin progression. This is reflected in a substantial

predicted ($12\,\text{cm}^{-1}$) drop in the frequency of ν_{30} as the D atom moves from the equatorial to the axial position (Table S1). If the minima are near $q_{37} = \pm 1$, a modelled, this implies a contribution to the linear term in the effective potential from ν_{30}, of $-3\,\text{cm}^{-1}\text{Å}^{-1}$ ($0.5 d\omega/dq$). But, from Equation 1, it is apparent that occupancy of $v_{30} = 1$ will triple the contribution of ν_{30} to the effective potential for q_{37}. As this contributes in the opposite sense to the overall zero-point energy correction, the effect is to flatten the potential and decrease the energy level spacing close to what is observed.

Modes ν_{35} and ν_{19} are not calculated to have a significant change in frequency between the axial and equatorial positions. This is reflected in the ν_{37} progression exhibiting spacings near identical to the origin. Mode ν_{23} is calculated to gain in frequency along q_{37}, yet we assign the spectrum to a spacing pattern similar to ν_{30}. This may point to a misassignment, but we also note that the calculated frequencies are very sensitive to the geometry and (TD)-B3LYP may not capture the full picture.

Finally, we note that several of the ionization efficiency spectra depicted in Figure 3 show structure above the first ionization onset. This is most apparent in the curves using band d_d as an intermediate state for 9D-An and the one using band h_a as an intermediate for 9H-An. For 9D-An this second onset appears $57\,\text{cm}^{-1}$ above the ionization threshold, while for 9H-An, the offset is almost double, $110\,\text{cm}^{-1}$. This spacing is again reminiscent of a low-frequency mode being excited in the cation which we surmise to be the equivalent to ν_{37} of the radical, the butterfly motion. We calculate that the cation ground state is C_{2v}. We postulate a low-frequency butterfly mode of around $60\,\text{cm}^{-1}$, where the $110\,\text{cm}^{-1}$ seen for 9H-An once again implies a $\Delta v = 2$ selection rule. The fact that this second ionization onset is most prominent for band d_d in Figure 3 can be rationalized with an appreciable geometry change along the butterfly mode upon ionization, which is also born out by the slow rising slope of the ionization spectrum for the origin band of 9D-An (d_a). The electronic excitation spectra of the closed-shell 9H-An$^+$ and

9D-An$^+$ cations will be reported in a future publication.

5   Conclusions

We report the excitation spectra and ionization efficiency curves of two isotopologues of the 9-dihydroanthracenyl radical. Both isotopologues were generated in our laboratory through an electric discharge of a seeded molecular beam containing anthracene vapor as well as normal and deuterated water for 9H-An and 9D-An, respectively. There is no evidence in our spectra for multiple isomers of either species, implying the lowest-energy isomer is exclusively formed and no isotope scrambling occurs in the deuterated species. The experimentally obtained value for the ionization energy of 9H-An is 6.3462(10) eV with the ionization energy of the deuterated isotopologue shifted by +0.001 eV.

Both isotopologues show clear evidence of substantial activity in the low-frequency "butterfly" motion. For 9D-An we observe additional bands in the butterfly progression compared to 9H-An. These bands are attributed to quantum-induced symmetry breaking of the deuterated isotopologue due to the difference in zero-point energy of the radical with the deuterium atom in the equatorial or axial positions.

Acknowledgements

References

[1] Manjavacas, A. *et al.* Tunable molecular plasmons in polycyclic aromatic hydrocarbons. *ACS Nano* **7**, 3635–3643 (2013).

[2] Mokkath, J. H. Optical properties of pyridine adsorbed polycyclic aromatic hydrocarbons using quantum chemical calculations. *Phys. Chem. Chem. Phys.* **21**, 448–454 (2019).

[3] Richter, H. & Howard, J. Formation of polycyclic aromatic hydrocarbons and their growth to soota review of chemical reaction pathways. *Prog. Ener. Combust. Sci.* **26**, 565–608 (2000).

[4] Johansson, K. O., Head-Gordon, M. P., Schrader, P. E., Wilson, K. R. & Michelsen, H. A. Resonance-stabilized hydrocarbon-radical chain reactions may explain soot inception and growth. *Science* **361**, 997–1000 (2018).

[5] Ravindra, K., Sokhi, R. & Van Grieken, R. Atmospheric polycyclic aromatic hydrocarbons: Source attribution, emission factors and regulation. *Atmos. Env.* **42**, 2895–2921 (2008).

[6] McGuire, B. A. *et al.* Detection of the aromatic molecule benzonitrile (c-C_6H_5CN) in the interstellar medium. *Science* **359**, 202–205 (2018).

[7] Tielens, A. Interstellar polycyclic aromatic hydrocarbon molecules. *Ann. Rev. Astron. Astrophys.* **46**, 289–337 (2008).

[8] Mennella, V., Hornekær, L., Thrower, J. & Accolla, M. The Catalytic Role of Coronene for Molecular Hydrogen Formation. *Astrophys. J.* **745**, L2 (2011).

[9] Page, V. L., Snow, T. P. & Bierbaum, V. M. Molecular Hydrogen Formation Catalyzed by Polycyclic Aromatic Hydrocarbons in the Interstellar Medium. *Astrophys. J.* **704**, 274–280 (2009).

[10] Foley, N. *et al.* Molecular hydrogen formation on interstellar PAHs through EleyRideal abstraction reactions. *Mon. Not. Roy. Astron. Soc.* **479**, 649–656 (2018).

[11] Hornekær, L., Baurichter, A., Petrunin, V. V., Field, D. & Luntz, A. C. Importance of surface morphology in interstellar H_2 formation. *Science* **302**, 1943–1946 (2003).

[12] Sandford, S. A., Bernstein, M. P. & Dworkin, J. P. Assessment of the interstellar processes leading to deuterium enrichment in meteoritic organics. *Meteor. Planet. Sci.* **36**, 1117–1133 (2001).

[13] Schmidt, T. W. The electronic spectroscopy of resonance-stabilised hydrocarbon radicals. *Int. Rev. Phys. Chem.* **35**, 209–242 (2016).

[14] Miller, J. A. & Klippenstein, S. J. The Recombination of Propargyl Radicals: Solving the Master Equation. *J. Phys. Chem. A* **105**, 7254–7266 (2001).

[15] Harding, L. B., Klippenstein, S. J. & Georgievskii, Y. On the Combination Reactions of Hydrogen Atoms with Resonance-Stabilized Hydrocarbon Radicals. *J. Phys. Chem. A* **111**, 3789–3801 (2007).

[16] Mebel, A. M. & Kaiser, R. I. Formation of resonantly stabilised free radicals via the reactions of atomic carbon, dicarbon, and tricarbon with unsaturated hydrocarbons: theory and crossed molecular beams experiments. *Int. Rev. Phys. Chem.* **34**, 461–514 (2015).

[17] Nakajima, M., Schmidt, T. W., Sumiyoshi, Y. & Endo, Y. Rotationally-resolved excitation spectrum of the jet-cooled cyclohexadienyl radical. *Chem. Phys. Lett.* **449**, 57–62 (2007).

[18] Wilcox, C. M., Krechkivska, O., Nauta, K., Schmidt, T. W. & Kable, S. H. Jet-cooled spectroscopy of ortho-hydroxycyclohexadienyl radicals. *J. Phys. Chem. A* **122**, 8886–8897 (2018).

[19] Lay, T. H., Bozzelli, J. W. & Seinfeld, J. H. Atmospheric Photochemical Oxidation of

Benzene: Benzene + OH and the Benzene-OH Adduct (Hydroxyl-2,4-cyclohexadienyl) + O_2. *J. Phys. Chem.* **100**, 6543–6554 (1996).

[20] Sebree, J. A., Kislov, V. V., Mebel, A. M. & Zwier, T. S. Spectroscopic and Thermochemical Consequences of Site-Specific H-Atom Addition to Naphthalene. *J. Phys. Chem. A* **114**, 6255–6262 (2010).

[21] Krechkivska, O. *et al.* Triple-Resonance Spectroscopy Reveals the Excitation Spectrum of Very Cold, Isomer-Specific Protonated Naphthalene. *J. Phys. Chem. Lett.* **4**, 3728–3732 (2013).

[22] Krechkivska, O. *et al.* H and D Attachment to Naphthalene: Spectra and Thermochemistry of Cold Gas-Phase 1-$C_{10}H_9$ and 1-$C_{10}H_8D$ Radicals and Cations. *J. Phys. Chem. A* **119**, 3225–3232 (2015).

[23] Sebree, J. A., Kislov, V. V., Mebel, A. M. & Zwier, T. S. Isomer specific spectroscopy of $C_{10}H_n$, n = 8-12: Exploring pathways to naphthalene in Titan's atmosphere. *Faraday Disc.* **147**, 231 (2010).

[24] Garkusha, I., Fulara, J., Nagy, A. & Maier, J. P. Electronic Absorption Spectra of Protonated Anthracenes and Phenanthrenes, and Their Neutrals in Neon Matrices. *Astrophys. J.* **728**, 131 (2011).

[25] Ivanov, S. D. *et al.* Quantum-induced symmetry breaking explains infrared spectra of CH_5^+ isotopologues. *Nat. Chem.* **2**, 298–302 (2010).

[26] Reilly, N. J. *et al.* Spectroscopic identification of the resonance-stabilized cis- and trans-1-vinylpropargyl radicals. *J. Amer. Chem. Soc.* **131**, 13423–13429 (2009).

[27] Chalyavi, N. *et al.* Excitation and Emission Spectra of Jet-Cooled Naphthylmethyl Radicals. *J. Phys. Chem. A* **115**, 7959–7965 (2011).

[28] O'Connor, G. D. *et al.* Excitation Spectra of Large Jet-Cooled Polycyclic Aromatic Hydrocarbon Radicals: 9-Anthracenylmethyl ($C_{15}H_{11}$) and 1-Pyrenylmethyl ($C_{17}H_{11}$). *J. Phys. Chem. A* **117**, 13899–13907 (2013).

[29] Nakagawa, K. & Itoh, N. Analysis of guesthost and intra-guest transitions for hydronaphthyl radicals in naphthalene crystals. *Chem. Phys.* **16**, 461–472 (1976).

[30] Chalyavi, N. *et al.* Spectroscopy and thermochemistry of a jet-cooled open-shell polyene: 1,4-pentadienyl radical **135**, 124306 (2011).

[31] Currie, C. L. & Ramsay, D. A. Electronic absorption spectrum and dissociation energy of the allyl radical. *J. Chem. Phys.* **45**, 488–491 (1966).

[32] Tsuge, M., Hamatani, S., Kawai, A., Tsuji, K. & Shibuya, K. Jet spectroscopy of arylmethyl radicals in the visible region: assignment of low-frequency vibrational modes in diphenylmethyl and chlorodiphenylmethyl radicals. *Phys. Chem. Chem. Phys.* **8**, 256–263 (2006).

[33] Krechkivska, O. *et al.* Ionization Energies of Three Resonance-Stabilized Radicals: Cyclohexadienyl (d_n, n = 0, 1, 6, 7), 1-Phenylpropargyl, and Methylcyclohexadienyl. *J. Phys. Chem. A* **118**, 10252–10258 (2014).

[34] Frisch, M. J. *et al.* Gaussian 16 Revision A.03 (2016). Gaussian Inc., 340 Quinnipiac Street, Building 40, Wallingford CT 06492.

[35] Troy, T. P. *The Spectroscopy of Radical Chromophores*. Ph.D. thesis, The University of Sydney (2011).

[36] Samanta, A., Bhattacharyya, K. & Chowdhury, M. Interaction of 2-pi electron systems - spectroscopy of 9,10-dihydroanthracene. *J. Phys. Chem.* **91**, 4671–4675 (1987).

[37] Chakraborty, T. & Chowdhury, M. Fluorescence excitation spectrum of jet-cooled dihydroanthracene. *Chem. Phys. Lett.* **171**, 25–28 (1990).

[38] Shin, Y. D., Saigusa, H., Zgierski, M. Z., Zerbetto, F. & Lim, E. C. Inversion potentials in the ground and excited states of 9,10-dihydroanthracene as probed by the absorption and excitation spectra of jet-cooled molecules. *J. Chem. Phys.* (199).

[39] Laane, J. Vibrational Potential Energy Surfaces and Conformations of Molecules in Ground and Excited Electronic States. *Ann. Rev. Phys. Chem.* **45**, 179–211 (1994).

[40] Verguilla-Berdecia, L. A. Tunneling in a quartic, symmetric, double well potential: A simple solution using a hermite basis. *J. Chem. Educ.* **70**, 928 (1993).